

## Waves and oscillations in plasma crystals

A Piel<sup>1</sup>, A Homann<sup>1</sup>, M Klindworth<sup>1</sup>, A Melzer<sup>1</sup>, C Zafiu<sup>1</sup>, V Nosenko<sup>2</sup>  
and J Goree<sup>2</sup>

<sup>1</sup> Institut für Experimentelle und Angewandte Physik, Christian-Albrechts-Universität Kiel,  
D-24098 Kiel, Germany

<sup>2</sup> Department of Physics and Astronomy, University of Iowa, Iowa City, IA 52242, USA

E-mail: piel@physik.uni-kiel.de

Received 5 September 2002, in final form 11 October 2002

Published 23 January 2003

Online at [stacks.iop.org/JPhysB/36/533](http://stacks.iop.org/JPhysB/36/533)

### Abstract

An overview of the properties of plasma crystals and clusters is given with emphasis on oscillations of particles in the plasma trap, instabilities associated with the solid–liquid phase transition and the propagation of waves. It is demonstrated how laser manipulation can be used to stimulate particle motion and waves. From characteristic resonance frequencies and from wave dispersion the particle charge and shielding length parameters, which determine the interparticle forces, can be quantitatively measured.

(Some figures in this article are in colour only in the electronic version)

### 1. Introduction

The formation of regular arrangements of charged particles (Wigner crystals) is well known from colloidal suspensions [1, 2] or laser-cooled ions in particle traps [3]. These systems have attracted much attention because of their beauty and their role as models for solid matter. Plasma crystallization, which was predicted by Ikezi in 1986 [4] and was experimentally established in 1994 [5–7] is the youngest member of this family. This field has experienced an exponential growth since then, which may be attributed to two peculiarities. The particles embedded in the plasma, which form the crystal at room temperature, are of micrometre size and can easily be observed with a macro lens. Moreover, because the particles are embedded in a low pressure gas discharge, dynamical processes of these particles are only weakly damped and occur at frequencies of a few tens of Hz and lower. Hence, complex dynamical phenomena can be analysed by following the individual particle motion with video microscopy. Most of these phenomena are not accessible in colloidal suspensions because of strong viscous damping.

There are many similarities but also significant differences between plasma crystals and Wigner crystals of laser-cooled ions. The most important difference is the neutralization of the space charge represented by the particles that form the crystal by the plasma ions. Therefore, plasma crystals are not subject to  $E \times B$  rotation, which is typical of ions in Penning

traps. Besides forming a neutralizing background, the ions are shielding the individual particle fields and modify the interaction potential between the embedded particles in the plasma, which deviates from a Coulomb law. As in colloidal suspensions, the pair interaction in the plasma crystal is often modelled by a Debye–Hückel (or Yukawa) potential.

The present paper is intended as a tutorial into the dynamic properties of plasma crystals, which manifest themselves as oscillations, waves and motion effects, which are either stimulated externally or are generated by internal processes. It is demonstrated that the radiation pressure of low power lasers is a suitable tool for stimulating these effects. The examples are chosen mostly from contributions of the Kiel group to this field of research. There are a number of recent reviews of the field of complex (dusty) plasmas and dynamic phenomena [8–11], which give credit to many researchers in this field and cover aspects that cannot be included here.

## 2. Oscillations of particles in the plasma trap

Charged particles of micrometre size cannot be trapped in homogeneous plasma regions, which are essentially field-free. Rather, under the influence of gravity, these particles sediment to the bottom of the plasma, where they are eventually levitated by strong electric fields in the space charge regions of the plasma boundary sheath [12].

### 2.1. Levitation of particles in radio-frequency discharges

The sheath of radio-frequency (rf) discharges in the geometry of a parallel plate etching reactor is particularly suitable for that purpose, because the time-averaged electric field shows a nearly linear dependence on position [13] (figure 1(a)). The inertia of the microparticles is so large that they do not follow the rf field at 13.56 MHz but react to the time averaged field only. The force balance in the levitation is governed by the electric field force and gravity:

$$Q_d E = M_d g, \quad (1)$$

$Q_d$  and  $M_d$  being the microparticles charge and mass. Other forces, like ion drag, neutral drag and thermophoresis, are negligible for micrometre size particles [14, 15]. The force balance resembles Millikan's famous oil drop experiments, but differs in the use of an inhomogeneous electric field here. Consequently, particles of different charge-to-mass ratio are levitated at different heights in the sheath. For small numbers of particles, each particle is free to move in its equilibrium plane in the sheath. At high particle densities, the mutual repulsion of the particles leads to the formation of multiple layers [16].

Lateral confinement of the particles in parallel plate reactors is usually accomplished by raising the equipotential contours by suitable metallic barriers such as copper gaskets or metal bars of a few millimetres thickness (figure 1(c)). This construction can be considered as a trap with confinement by surface forces. The particles are illuminated with a sheet of laser light and observed from the top or from the side with a video camera. Confinement by volume forces (in 2D) can be realized by giving the electrode a concave shape (figure 1(b)). Then, the equipotential contours become approximately parabolic and a radial electric field is generated that increases linearly from the centre to the edge.

### 2.2. The resonance method

The linear dependence of the vertical confining field on position together with gravity results in an effective harmonic potential well, in which the microparticles are trapped. This potential

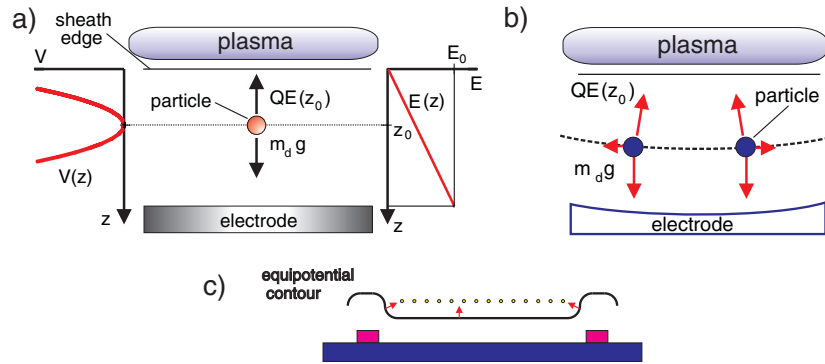


**Figure 1.** (a) Levitation of negatively charged particles by the inhomogeneous electric field in the plasma sheath region. (b) Curved equipotential contours give rise to radial confinement of the particles. (c) Raising the equipotentials by barriers on the electrode for confinement of particles by surface forces.

well has an eigenfrequency for vertical oscillations, which is related to the charge-to-mass ratio  $Q_d/M_d$  of the particles and the plasma ion density  $n_i$ :

$$\omega_v^2 = \frac{Q_d n_i e}{M_d \epsilon_0}. \tag{2}$$

$\epsilon_0$  is the permittivity of free space. We have used this resonance as a method for determining the charge on the microparticles [17, 18]. This method is sufficiently accurate for particles of well-known mass. For this reason and for studying the interaction of identical particles, most experiments on plasma crystals are made with monodisperse spherical plastic particles. At about  $10 \mu\text{m}$  diameter a charge of  $Q = -14\,000e$  is found. The resonance can be excited by applying an additional low-frequency voltage to the lower electrode of the rf discharge, which leads to a periodic vertical shift of the equilibrium position. Later, we had refined this technique by exciting vertical oscillations of individual particles with the radiation pressure of a periodically chopped laser [19]. Typical resonance curves for both methods of excitation are shown in figure 2(a). The main resonance appears at about 15 Hz, while a spurious resonance near 5 Hz corresponds to excitation of the main resonance with the harmonics contained in the square wave force of the chopped laser. This effect is verified by applying a square wave voltage to the electrode.

### 2.3. Nonlinear oscillations and parametric effects

For high excitation voltages, the vertical resonance shifts towards lower frequencies. The nonlinear resonance curve (figure 2(b)) shows the typical hysteresis of driven nonlinear oscillators. The downshift of the resonance is an immediate hint at the softening of the potential energy curve at high amplitudes. For the upward motion, an average reduction of the restoring force can be expected from the fact that the particles begin to penetrate into the quasi-neutral plasma. For the downward motion, the potential energy curve flattens because of a reduction of the particle charge. Microparticles are charged by the balance between electron and ion flow towards the particle. In homogeneous plasmas the higher electron mobility leads to the high negative charge of the microparticles. In the sheath region, the time averaged electron concentration rapidly drops from the plasma edge towards the electrode. This drop is much faster than the drop of ion density. Hence, the collection of negative charge becomes

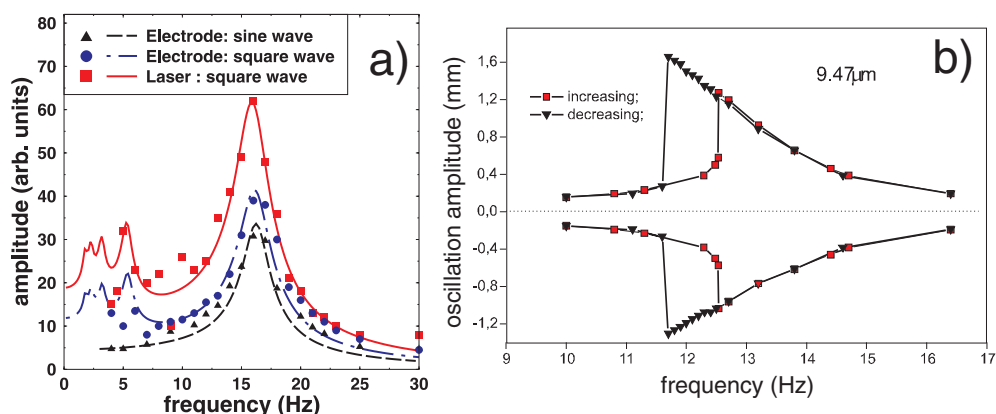


**Figure 2.** (a) Vertical resonance of trapped particles for laser excitation or excitation with a periodic bias voltage on the electrode. For square wave excitation, spurious resonances appear at  $1/3$  and  $1/5$  of the fundamental frequency. (b) Nonlinear resonance curve and hysteresis for high excitation voltage.

less efficient on the lower half of the particle trajectory. These arguments are supported by a careful model analysis [20].

Oscillations of particles in the plasma trap can also be stimulated by introducing a fine wire into the trap, which is biased with a suitable periodic voltage. The bias voltage of the wire has two effects. First, there is an immediate field force on the adjacent particles, which leads to particle motion. Second, the particle trap is slightly distorted and leads to a periodic oscillation of the confinement parameters. We could show that the vertical resonance of the microparticles can be excited at twice the fundamental frequency of the potential well. This excitation has the characteristic properties of a parametric resonance. The excitation amplitude has to exceed a threshold value and this threshold shifts towards higher values when the frictional damping is increased [21]. When using excitation of particle motion or oscillations with biased wires, one has to bear in mind that the spatial distribution of the force is not well defined and that unwanted side effects can occur by the unavoidable distortion of the plasma trap.

### 3. Small clusters

A specific class of plasma crystals is the formation of small two-dimensional clusters containing less than 100 particles. These clusters are confined by the force generated by a parabolic shaped electrode (figure 1(c)). This kind of particle trap gives a radially parabolic confining potential, which has been studied theoretically in great detail [22, 23]. The particles are found to be arranged in regular patterns, which obviously follow the principle of filling subsequent shells [24]. Because of the similarity to the shell structure of charged particle arrangements in a homogeneous space charge cloud, which provides a 3D parabolic particle trap and was used by Thomson as an early model of an atom [25], the small clusters are often referred to as ‘artificial atoms’.

Clusters with certain ‘magic’ numbers of particles represent particularly stable configurations, among them the system with 19 particles and configuration (1–6–12). The six-fold symmetry and the commensurate number of particles in the outer shell is responsible for the stability. The neighbouring system ( $N = 20$ , (1–7–12)) has a mismatch between the inner and outer ring. The lowest excited state of these systems is an intershell rotation between

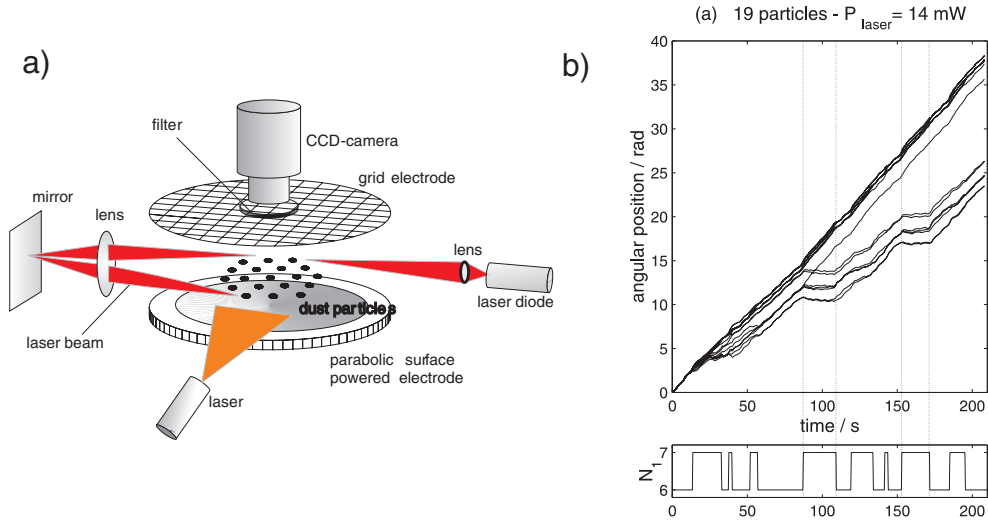


**Figure 3.** (a) Experimental set-up for generating a torque on a 19-particle cluster. (b) Stick-slip motion of particles in the inner ring by a structural transition becomes evident from the phase evolution of all 19 particles. Particles in the inner ring are decoupled from the outer ring ('slip phase') when the configuration changes from (1-6-12) to (1-7-11).

the outer and inner ring. Klindworth *et al* [26] have excited this mode with a pair of laser beams that exerts a torque on the outer ring (figure 3(a)). The  $N = 20$  cluster easily performs this intershell rotation while the  $N = 19$  cluster either performs rigid rotation of the entire cluster or performs a structural transition to a (1-7-11) configuration that allows for intershell rotation (figure 3(b)). This structural change is an example of how the transition from sticking friction to gliding friction works at the atomic scale.

#### 4. Plasma crystals

A dense arrangement of highly charged microparticles reaches a state of strong coupling and forms a Coulomb liquid or solid. The system is characterized by the coupling strength

$$\Gamma = \frac{Q_d^2}{4\pi\epsilon_0 b k T}. \quad (3)$$

$\Gamma$  is the ratio of the potential energy of nearest neighbours at the mean interparticle distance  $b$  to the thermal energy  $kT$ . In plasmas, the interaction potential deviates from a Coulomb law by shielding effects, which are described by the shielding factor

$$\kappa = b/\lambda_D \quad (4)$$

where  $\lambda_D$  is the Debye shielding length [27]. Depending on the number of injected particles, single-layer crystals, two-layer crystals or multilayer crystals with up to 10–15 layers can be formed. The crystal structure is hexagonal in the plane (figure 4(a)) but often forms vertically aligned particle strings (figure 4(b)) [28]. Crystal structures that are more typical of three-dimensional extended crystals (fcc, bcc and hcp) have been reported by other authors [29] at high gas pressures, where the mechanism for string formation is destroyed.

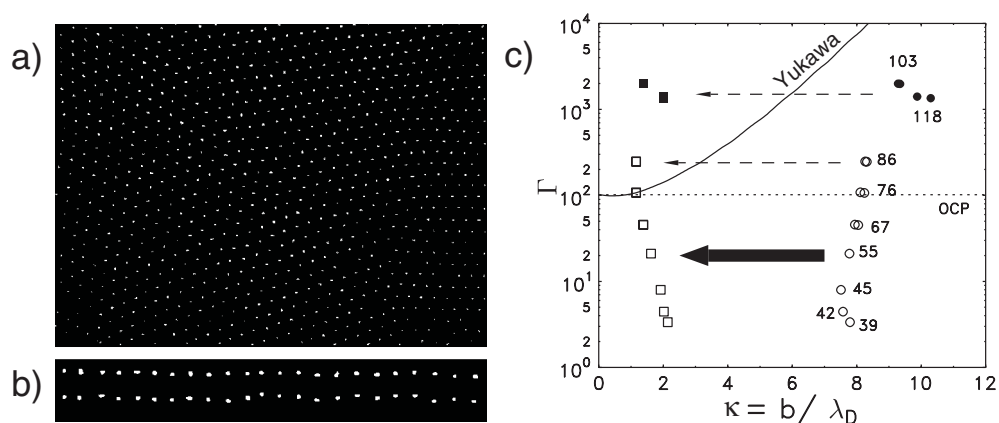


**Figure 4.** (a) Top view of a plasma crystal with hexagonal structure. (b) The side view of a two-layer crystal shows vertical alignment of the particles. (c) Comparison of the melting line with experimental data from a two-layer crystal (see text). The data points are labelled with the corresponding gas pressure (Pa).

#### 4.1. Solid–liquid phase transition

There was much interest in the solid–liquid phase transition of plasma crystals, which were considered, besides colloidal suspensions, as a suitable model system for two-dimensional melting [30–32]. Melzer *et al* [28] had observed that reducing the gas pressure in the rf discharge leads to a solid–liquid phase transition in two-layer crystals. Single-layer crystals did not perform this phase transition. The phase transition is accompanied by low-frequency precursor oscillations of the vertically aligned particle pairs. Similar observations were reported by Thomas and Morfill [33] who described the liquid state as a ‘flue and flow’ state and also identified a ‘vibrational state’. The first quantitative comparison of the measured values for  $\Gamma$  and  $\kappa$  with a phase diagram [28] is shown in figure 4(c). For  $\kappa \rightarrow 0$  the Yukawa model approaches the limit of the one-component-plasma (OCP) model. Full symbols represent crystalline states, open symbols fluid states. The squares use the measured shielding factors from coupled oscillations [34] whereas the circles were based on shielding by thermal ions. The squares evidently give the better agreement with the Yukawa melting line.

In general, the melting phase transition was found not to follow the Kosterlitz–Thouless scenario [30–32] with the formation of an intermediate hexatic phase. Rather, the phase transition was closer to a first-order transition.

#### 4.2. The Schweigert instability

The remarkable difference between the melting of the two-layer crystal and the stability of single-layer crystals was resolved by the discovery of a novel type of plasma instability [35, 36]. This model starts from the fact that the plasma sheath, where the crystal forms, sustains a supersonic ion flow from the plasma to the electrode. This flow is deflected by the highly charged grains and leads to charge accumulation in the wake of the particles [37, 38]. The main assumption of the model is that this positive net charge exerts an attractive force on the particles in the lower layer but that this force is asymmetric. In its simplest form, the Schweigert instability can be understood in terms of two coupled linear chains of particles, in which the particles interact by short-range repulsive forces [28]. The two chains are coupled

by repulsive and asymmetric attractive forces:

$$\begin{aligned}\ddot{x}_1^{(n)} + \nu\dot{x}_1^{(n)} &= \frac{k_1}{m}(x_1^{(n-1)} - 2x_1^{(n)} + x_1^{(n+1)}) + R(x_1^{(n)} - x_2^{(n)}) \\ \ddot{x}_2^{(n)} + \nu\dot{x}_2^{(n)} &= \frac{k_2}{m}(x_2^{(n-1)} - 2x_2^{(n)} + x_2^{(n+1)}) - R(x_1^{(n)} - x_2^{(n)}) + A(x_1^{(n)} - x_2^{(n)}).\end{aligned}\quad (5)$$

$k_1, k_2$  are the ‘spring constants’ in the upper/lower chain, and  $R$  and  $A$  are the repulsive and attractive coupling between the chains, respectively. The asymmetric attractive force leads to complex roots of the characteristic polynomial, which correspond to self-excited waves. These waves only appear below a threshold of the friction coefficient. This simple model gives a quantitative prediction of the critical gas pressure for the onset of spontaneous precursor oscillations and for the frequency of unstable modes. Both agree with experiment.

### 4.3. Attractive forces

The existence of attractive forces that lead to vertical alignment of particles was demonstrated by laser manipulation of particle chains [39] and ‘dust molecules’ [40, 41]. In the latter experiment two particles of slightly different mass formed a vertically aligned pair. When the upper particle was pushed sideways the lower particle strictly followed the upper particle’s motion. However, when the lower particle was pushed by the same laser force the binding with the upper particle was destroyed. This clearly demonstrates the asymmetric nature of the attractive force. The asymmetry is attributed to the symmetry breaking by the supersonic ion flow, which allows information (ion acoustic waves) to be communicated downstream but not upstream. It is worth remembering that attractive forces by polarization of the background medium account for the binding of Cooper pairs in superconductors.

## 5. Waves in plasma crystals

Solid matter can support two types of sound waves, longitudinal (compressional) and transverse (shear) waves, with different propagation velocities. Both sound velocities depend on the particle charge but have a different functional dependence on the shielding parameter  $\kappa$  [42]. The sound speed  $c_L, c_T$  for the longitudinal and transverse dust lattice wave, respectively, can be written (in the absence of damping and thermal effects) as [42–44]

$$c_{L,T} = \lim_{q \rightarrow 0} \frac{\partial \omega_{L,T}}{\partial q} = \lim_{q \rightarrow 0} \frac{\omega_{L,T}}{q} = \left( \frac{Q_d^2}{4\pi\epsilon_0 M_d b} \right)^{1/2} c_{L,T}^*(\kappa). \quad (6)$$

The factor  $c_{L,T}^*$  is a normalized sound speed for longitudinal and transverse waves in 2D systems:

$$c_L^*(\kappa) = \left( \sum_R \frac{1}{R} \exp(-R\kappa) \left[ \frac{15}{8}(1 + R\kappa) + \frac{9}{8}R^2\kappa^2 \right] \right)^{1/2} \quad (7)$$

$$c_T^*(\kappa) = \left( \sum_R \frac{1}{R} \exp(-R\kappa) \left[ -\frac{3}{8}(1 + R\kappa) + \frac{3}{8}R^2\kappa^2 \right] \right)^{1/2}. \quad (8)$$

Here, the sum is over all possible interparticle distances  $R = r_{ij}/b$  in a hexagonal lattice. Sound waves have been used as a suitable tool for the diagnostics of plasma crystals.

### 5.1. Compressional and shear waves

The compressional dust lattice wave [45] was studied experimentally in one-dimensional [46] and two-dimensional [47] plasma crystals with excitation by chopped laser radiation.

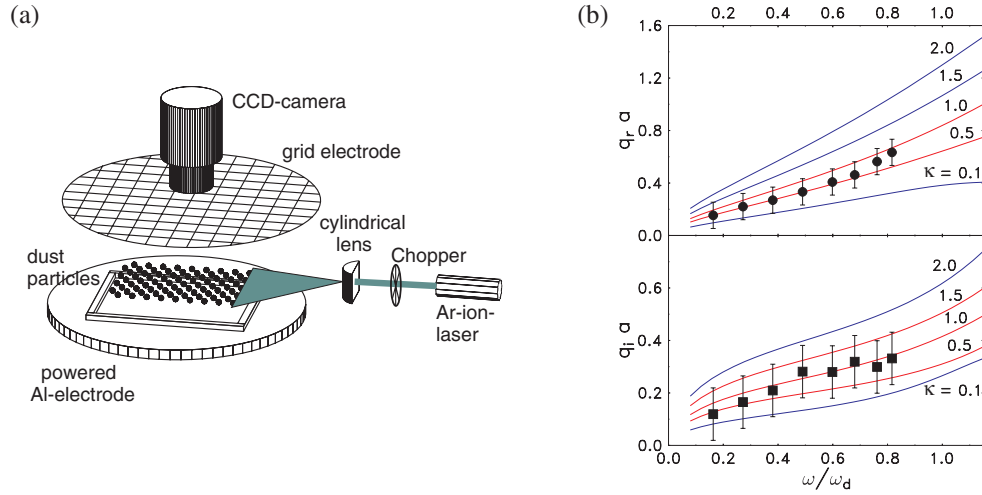


**Figure 5.** (a) Experimental arrangement for exciting a plane compressional wave in a single-layer plasma crystal. (b) Real and imaginary parts of the wavenumber as a function of excitation frequency. Theoretical curves are given for various values of  $\kappa$ .

Figure 5(a) shows the typical arrangement for excitation of plane waves in a 2D crystal. Single-layer crystals are used to avoid melting by the Schweigert instability. The wavefront and the laser force are at right angles to excite the compressional mode. The compressional wave propagates as a damped wave into the plasma crystal. From the motion of individual particles between successive video frames the local wave amplitude and phase are determined. The resulting real and imaginary parts of the wavenumber are shown in figure 5(b) in comparison with theoretical curves for various values of the shielding factor  $\kappa$ . The resulting shielding factor was  $\kappa = (0.8 \pm 0.4)$ .

The excitation of plane shear waves was likewise achieved with a laser fan that illuminated a row of particles that is aligned with the laser force direction [48]. A shear wave pulse separated at right angles from the initially perturbed region and was found to propagate at the sound velocity for shear waves. The resulting wave velocity was compatible with  $Q_d = -12\,000e$  and  $0 < \kappa < 1.4$ .

## 5.2. Mach cones

A supersonic object in a liquid or gas is known to create a Mach cone, which is the envelope of circular waves radiated from sharp edges of the object. Samsonov *et al* [49, 50] observed that fast moving particles in a plane below a single-layer plasma crystal can excite Mach cones in a solid that are formed by lattice waves. This work was extended by exciting Mach cones with a moving laser spot [44]. The half-angle  $\theta_c$  of the Mach cone obeys the relationship

$$\sin(\theta_c) = c_L/v \quad (9)$$

where  $v$  is the velocity of the perturbing object or laser spot. Mach cones were originally suggested as a diagnostic means for the dusty plasma in Saturn's ring [51], which may be observed when the Cassini spacecraft arrives there in 2004.

The Mach cones in plasma crystals possess an interesting multiple structure of nested cones, which were explained as dispersive effects of compressional waves [52]. The phenomenon is similar to the internal structure of Kelvin wedges that form in ship waves.

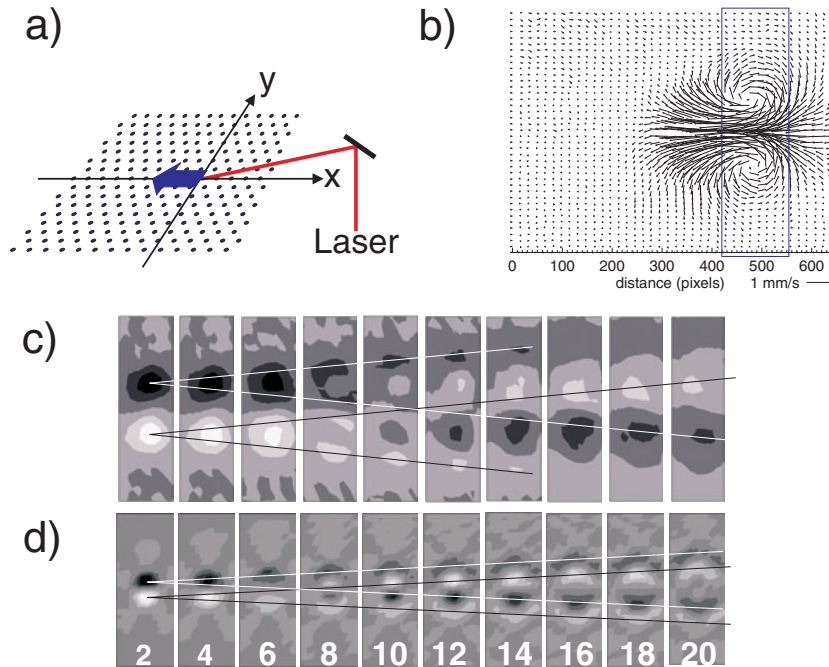


**Figure 6.** (a) Geometry for simultaneous excitation of compressional and shear waves in a single-layer plasma crystal with a point dipole. (b) Velocity vector field at the end of the laser pulse. (c) The vorticity of the measured velocity field reveals the evolution of vortex–antivortex pairs. (d) Molecular dynamics simulation of the shear wave in the same representation. The frame number of the video at 30 fps is indicated.

Recently, it was demonstrated that pure shear wave Mach cones can be excited, when  $c_L > v > c_T$  [53]. When the laser spot velocity is higher than both sound velocities, even a nested set of a compressional and a shear wave Mach cone was observed.

### 5.3. Radiation from a localized source

While there is now ample knowledge about the propagation of plane waves or Mach cones far from the excitation region, the radiation field close to the excitation region still needs particular attention. This problem was studied experimentally with a laser force that caused a localized shear stress in the plasma crystal [54]. Figure 6(a) shows the excitation geometry and figure 6(b) the initial perturbation. The full velocity field and its temporal evolution can be derived from the video microscopy. A complicated, elastic double vortex structure emanates from the excitation region. The two fundamental wave types that make up this complicated wave pattern can be separated because the longitudinal mode is irrotational and the shear wave is area preserving. Hence, taking the divergence of the velocity field projects on the compressional mode. Likewise, the vorticity  $\nabla \times \vec{v}$  of the velocity field represents the shear wave activity. The evolution of the shear wave (figure 6(c)) is characterized by an initial double vortex. Each of the vortices splits into an outgoing and inward-going vortex. The inward-going structures show a crossover in the centre of excitation and reappear as a secondary outgoing vortex that follows the original outgoing vortex. Hence, the final wave field is again a pair of vortex–antivortex propagating at the sound velocity of the shear wave. The wavefronts are circular about the source region. The angular distribution of radiation intensity resembles the

$\cos^2 \alpha$  law of dipole radiation. Figure 6(d) shows the same evolution of the shear wave from a molecular dynamics simulation, which confirms all mentioned details.

The compressional wave also forms circular wavefronts, although with an orthogonal distribution of radiation energy. The compressional wave, which starts as a pair of compression and rarefactive pulses, also splits into inward-going and outward-going structures. Different from the shear wave, the compressional wave evolves into a wave train. We attribute this difference to the nearly dispersionless character of the shear, while the compressional wave possesses substantial dispersion, which leads to the multiple Mach cone structures mentioned above. Hence, the wave train formation and the Mach cone structure are two manifestations of the same phenomenon.

## 6. Conclusions

Waves and oscillations have been widely used as a reliable diagnostic tool for plasma crystals. They yield the particle charge  $Q_d$  and the shielding factor  $\kappa$  and have led to a quantitative understanding of the interparticle forces. In several examples the manipulation of particles and excitation of waves with low-power lasers was illustrated, which has now become a well established method.

## Acknowledgments

This work was supported by DFG grants Pi185/8-1, /8-2, /17-1, /21-1 and by INTAS grant 97-0775.

## References

- [1] Clark N A, Hurd A J and Ackerson B J 1979 *Nature* **281** 57–60
- [2] Pieranski P 1983 *Contemp. Phys.* **24** 25–73
- [3] Wineland D J, Bergquist J C, Itano W M, Bollinger J J and Manney C H 1987 *Phys. Rev. Lett.* **59** 2935–8
- [4] Ikezi H 1986 *Phys. Fluids* **29** 1764–6
- [5] Chu J H and I L 1994 *Physica A* **205** 183–90
- [6] Hayashi Y and Tachibana K 1994 *Japan. J. Appl. Phys.* **33** L804–6
- [7] Thomas H, Morfill G E, Demmel V, Goree J, Feuerbacher B and Möhlmann D 1994 *Phys. Rev. Lett.* **73** 652–5
- [8] Merlino R L, Barkan A, Thompson C and D'Angelo N 1998 *Phys. Plasmas* **5** 1607–14
- [9] Melzer A 2001 *Plasma Sources Sci. Technol.* **10** 303–10
- [10] Shukla P K 2001 *Phys. Plasmas* **8** 1791–803
- [11] Piel A and Melzer A 2002 *Plasma Phys. Control. Fusion* **44** R1–26
- [12] Selwyn G S, Heidenreich J E and Haller K L 1991 *J. Vac. Sci. Technol. A* **9** 2817–24
- [13] Tomme E B, Law D A, Annaratone B M and Allen J E 2000 *Phys. Rev. Lett.* **85** 2518–21
- [14] Jellum G M and Graves D B 1990 *Appl. Phys. Lett.* **57** 2077–9
- [15] Barnes M S, Keller J H, Forster J C, O'Neill J A and Coultas D K 1992 *Phys. Rev. Lett.* **68** 313–16
- [16] Dubin D 1993 *Phys. Rev. Lett.* **71** 2753–6
- [17] Melzer A, Trottenberg T and Piel A 1994 *Phys. Lett. A* **191** 301–8
- [18] Trottenberg T, Melzer A and Piel A 1995 *Plasma Sources Sci. Technol.* **4** 450–8
- [19] Homann A, Melzer A and Piel A 1999 *Phys. Rev. E* **59** 3835–8
- [20] Zafiu C, Melzer A and Piel A 2001 *Phys. Rev. E* **63** 066403
- [21] Schollmeyer H, Melzer A, Homann A and Piel A 1999 *Phys. Plasmas* **6** 2693–8
- [22] Bedanov V M and Peeters F 1994 *Phys. Rev. B* **49** 2667–76
- [23] Schweigert V A 1995 *Pis. Zh. Tech. Fis.* **21** 69 (Engl. transl. 1995 *Tech. Phys. Lett.* **21** 476)
- [24] Lai Y J and I L 1999 *Phys. Rev. E* **60** 4743–53
- [25] Thomson J J 1904 *Phil. Mag.* **39** 236
- [26] Klindworth M, Melzer A, Piel A and Schweigert V A 2000 *Phys. Rev. B* **61** 8404–10
- [27] Robbins M O, Kremer K and Grest G S 1988 *J. Chem. Phys.* **88** 3286–312

- [28] Melzer A, Homann A and Piel A 1996 *Phys. Rev. E* **53** 2757–66
- [29] Pieper J, Goree J and Quinn R 1996 *J. Vac. Sci. Technol. A* **14** 519–20
- [30] Kosterlitz J M and Thouless D J 1973 *J. Phys. C: Solid State Phys.* **6** 1181–203
- [31] Nelson D R and Halperin B I 1979 *Phys. Rev. B* **19** 2457–84
- [32] Young A P 1979 *Phys. Rev. B* **19** 1855–66
- [33] Thomas H and Morfill G E 1996 *Nature* **379** 806–9
- [34] Peters S, Homann A, Melzer A and Piel A 1996 *Phys. Lett. A* **223** 389–93
- [35] Schweigert V A, Schweigert I V, Melzer A, Homann A and Piel A 1996 *Phys. Rev. E* **54** 4155–66
- [36] Melzer A, Schweigert V, Schweigert I, Homann A, Peters S and Piel A 1996 *Phys. Rev. E* **54** R46–9
- [37] Nambu M, Vladimirov S V and Shukla P K 1995 *Phys. Lett. A* **203** 40–2
- [38] Melandsø F and Goree J 1995 *Phys. Rev. E* **52** 5312–26
- [39] Takahashi K, Oishi T, Shimomai K, Hayashi Y and Nishino S 1998 *Phys. Rev. E* **58** 7805–11
- [40] Melzer A, Schweigert V A and Piel A 2000 *Phys. Scr.* **61** 494–501
- [41] Melzer A 2001 *Phys. Scr.* **89** 33–6
- [42] Peeters F M and Wu X 1987 *Phys. Rev. A* **35** 3109–14
- [43] Wang X, Bhattacharjee A and Hu S 2001 *Phys. Rev. Lett.* **86** 2569–72
- [44] Melzer A, Nunomura S, Samsonov D and Goree J 2000 *Phys. Rev. E* **62** 4162–76
- [45] Melandsø F 1996 *Phys. Plasmas* **3** 901
- [46] Homann A, Melzer A and Piel A 1996 *Phys. Bl.* **52** 1227–31
- [47] Homann A, Melzer A, Peters S, Madani R and Piel A 1997 *Phys. Rev. E* **56** 7138–41
- [48] Nunomura S, Samsonov D and Goree J 2000 *Phys. Rev. Lett.* **84** 5141–4
- [49] Samsonov D, Goree J, Ma Z, Bhattacharjee A, Thomas H M and Morfill G E 1999 *Phys. Rev. Lett.* **83** 3649–52
- [50] Samsonov D, Goree J, Thomas H M and Morfill G E 2000 *Phys. Rev. E* **61** 5557–72
- [51] Havnes O, Aslaksen T, Hartquist T W, Li F, Melandsø F, Morfill G E and Nitter T 1995 *J. Geophys. Res.* **100** 1731–4
- [52] Dubin D H E 2000 *Phys. Plasmas* **7** 3895–903
- [53] Nosenko V, Goree J, Ma Z W and Piel A 2002 *Phys. Rev. Lett.* **88** 135001
- [54] Piel A, Nosenko V and Goree J 2002 *Phys. Rev. Lett.* **89** 085004